PHYSICAL REVIEW B VOLUME 13, NUMBER 10 15 MAY 1976

Metal-semiconductor junction for (110) surfaces of zinc-blende compounds

E. Louis, F. Yndurain,* and F. Flores
Centro Coordinado de Física, C-12 6°, Universidad Autónoma, Canto Blanco, Madrid 34, Spain
(Received 24 February 1975)

The behavior of the metal-semiconductor junction is studied for some III–V and II–VI zinc-blende compounds, within the framework of a one-electron theory. Using a pseudopotential description of the semiconductor crystals, the density of interface states is analyzed performing the matching of the wave functions at the interface. The characteristics of the different types of interface states are discussed in detail, and particular examples are given for contacts with metals of high and low electronic densities. As a by-product, the surface states at the semiconductor vacuum interface are also calculated. Finally, the barrier potential of the junction is obtained as a function of the metal work function (for metals of high density). Although very good agreement has been found with the experimental data for the compounds of the covalent group, large discrepancies arise for those of the ionic group. Some comments on the reasons for these discrepancies are made.

I. INTRODUCTION

The metal-semiconductor (M-S) interface is of prime interest not only because of its technical applications,[1] but also owing to other theoretical and experimental reasons; for instance, the study of the properties of the M-S junction could help one attain a better understanding of the characteristics of the junction components. In particular, the M-S interface has recently been used[2] to study the ionic character of dielectric crystals. It turns out, after the analysis of the experimental data carried out by Kurtin *et al.*,[2] that the dielectric crystals could be classified into two main groups, ionic and covalent, according to the degree of stability of the Fermi level when the crystal is placed in intimate contact with different metals. The more ionic the crystal, the weaker the pegging of the Fermi level, and the junction has a more Schottky-like[1] behavior. On the other hand, in the extreme covalent case the Fermi level is pegged by a high density of interface states[3] that confers a Bardeen-like behavior[1] to the contact. Moreover, this transition from Schottky to Bardeen-like behavior seems to occur abruptly. This striking transition is explained by Kurtin *et al.*[2] in terms of the electronic differences between the valence-band states of those two groups; namely, in the covalent crystals the valence states have an extended character, while in the ionic solids this character is localized.

In a previous paper[4] we reported the preliminary results of a study of the behavior of some zinc-blende solids at the M-S interface; we studied just the (110) surface of those crystals. At this stage our purpose is to describe and extend the model and calculations we performed in I. We shall investigate the role played by the interface states in the M-S junction of (110) surfaces of zinc-blende crystals and whether the transition outlined above can be explained in terms of those interface states.

Our model is mainly based upon a pseudopotential description of the semiconductor bulk band structure. Although we shall perform the calculation using the abrupt potential model (APM), we shall discuss, by means of a model previously applied to the semiconductor-vacuum system,[5] the relevance of a smooth interface potential at the M-S junction. The density of interface states is analyzed by performing the matching of the wave functions at the interface; in the present work we analyze two points of high symmetry of the two-dimensional Brillouin zone (BZ). The characteristics of the different types of interface states[3] which can appear at the M-S junction are discussed in detail and particular examples are given for contacts with metals of high and low electronic densities. Detailed calculations are performed for some zinc-blende crystals joined to a metal of high density (Al); our results confirm the conclusions of I (that calculation was carried out considering a single point of the BZ) in the sense that while our theoretical calculation agrees with the available experimental data for solids of the covalent group, the differences between the theoretical and the experimental results for crystals of the ionic group are remarkable. At the end of this paper we shall discuss these discrepancies.

As the most important by-product of our analysis, we shall study the semiconductor-vacuum interface; this study will be a way of checking our description of the semiconductor wave functions by comparing our results for the surface-state energies with those obtained by means of more elaborate calculations.[6] Our analysis allows us to write secular equations for the surface-state energies which consider in a clear way the heteropolar character of the (110) surface of the zinc-blende structure.

This paper is organized as follows: In Sec. II we shall present the calculation of the evanescent wave functions at two points of the BZ, which we

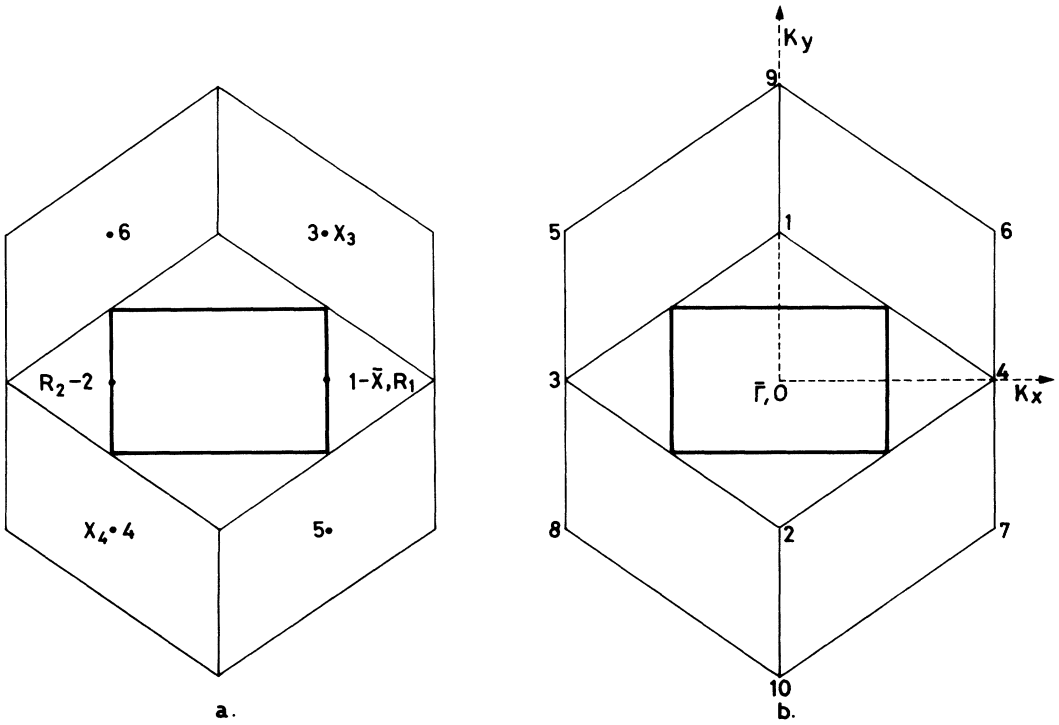

FIG. 1. Two-dimensional BZ (inner rectangle) and projected Jones zone for the (110) face of a fcc lattice. The parallel components of the crystal momentum which were included in the analysis of the $\bar{\Gamma}$ and $\bar{X}$ points of the two-dimensional BZ are shown in (a) and (b), respectively.

have carried out in an analytical way, with a description of the approximations involved in our analysis; in Sec. II we also calculate the surface-state energies at the free surface of seven zinc-blende crystals. In Sec. III the characteristics of the interface states at the M-S junction are studied for the two points of the BZ analyzed in Sec. II. Although the detailed calculation of interface states is restricted to metals of high electronic density, the junctions with a metal of low density (Na) are also discussed and some details of the interface states which can be found, are given. The relevance of the interface potential in the calculation of interface states is also discussed. In Sec. IV we apply the analysis of Sec. III to the quantitative study of the barrier height at the M-S interface for the (110) surface of seven zinc-blende crystals; our results are discussed and compared with the available experimental data.[2] Finally, in Sec. V we make some concluding remarks.

II. EVANESCENT WAVE FUNCTIONS AT (110) ZINC-BLENDE SURFACES: SURFACE STATES

In this section we shall study analytically the semiconductor wave function at the forbidden energy region. We shall base our analysis on the pseudopotential scheme; in particular, we shall take the pseudopotential form factors from the empirical pseudopotential method.[7]

In principle, the exact study of the matching process at the interface would require including an infinite set of evanescent waves in correspondence to the infinite number of parallel components of the crystal momentum associated with a given $\vec{\kappa}$ of the first two-dimensional BZ.[8] Unfortunately, since we cannot get an infinite set of waves to be matched, we must take a finite number of evanescent functions. As discussed elsewhere,[9] an essential requirement for an approximation to give physically sensible results is that the number of real lines must equal the number of parallel reciprocal-lattice vectors used in the calculation. In order to satisfy the above requirement we shall use here the method employed by Elices *et al.*[9] As discussed by these authors, the evanescent waves at the (111) surface of silicon can be described with enough accuracy by including in the analysis of a particular $\vec{\kappa}$ of the BZ just those parallel components lying inside the (111) projection of the Jones zone.[10,11] In this section we shall use that criterion for studying the evanescent waves at two points of high symmetry of the BZ ($\bar{\Gamma}$ and $\bar{R}$,[12] see Fig. 1).

A. Point $\bar{R}$

Consider the point $R_1(\frac{1}{2}, \frac{3}{2}, 0)$ of the three-dimensional bulk band structure. As one moves along

the [110] direction, one comes across three other points of this symmetry, $(0,1,0)$, $(\bar{\frac{1}{2}},\frac{1}{2},0)$, and $(\bar{1},0,0)$, respectively, equivalent to $X_4(1,0,\bar{1})$, $R_2(\frac{3}{2},\frac{1}{2},0)$, and $X_3(0,1,1)$ [Fig. 1(a)]. As sketched in Fig. 1(a), at the point R_1 we have the following six parallel components of the crystal momentum lying inside the (110) projection of the Jones zone[13]:

$$|\vec{\kappa}_1\rangle=(\tfrac{1}{2}\sqrt{2},0)\ ,\quad |\vec{\kappa}_4\rangle=(\tfrac{1}{2}\sqrt{\bar{2}},\bar{1})\ ,$$
$$|\vec{\kappa}_2\rangle=(\tfrac{1}{2}\sqrt{\bar{2}},0)\ ,\quad |\vec{\kappa}_5\rangle=(\tfrac{1}{2}\sqrt{2},\bar{1})\ , \tag{1}$$
$$|\vec{\kappa}_3\rangle=(\tfrac{1}{2}\sqrt{2},1)\ ,\quad |\vec{\kappa}_6\rangle=(\tfrac{1}{2}\sqrt{\bar{2}},1)\ .$$

We shall describe the bulk band structure at X_3 by means of the six plane waves

$$\begin{array}{cccccc}(0,1,1) & (0,\bar{1},1) & (0,\bar{1},\bar{1}) & (0,1,\bar{1}) & (1,0,0) & (\bar{1},0,0)\\ |\vec{\kappa}_3\rangle & |\vec{\kappa}_6\rangle & |\vec{\kappa}_4\rangle & |\vec{\kappa}_5\rangle & |\vec{\kappa}_2\rangle & |\vec{\kappa}_1\rangle\end{array} \tag{2}$$

which have the parallel components indicated in (2). These waves are only those included by Heine and Jones[14] in their study of the bulk band structure of diamond crystals. In order to find the real lines and evanescent wave functions at this point, we add $\lambda(110)=\lambda\vec{h}$ to each one of the plane waves of (2).

For energies in the principal forbidden gap we find two loops joining through the complex $\vec{\kappa}$ plane the valence-band level E_5 with the conduction levels E_1 and E_3. In diamond crystals[15,16] E_1 and E_3 are degenerate, giving rise to a single degenerate loop. The following wave function is associated to the first loop [in components of the plane waves in (2)]:

$$\phi_1=e^{-q_1 z}[(i,1,0,0,\tfrac{1}{2}(1+i)\alpha_4,\tfrac{1}{2}(1-i)\alpha_4) + a_1(0,0,-i,1,\tfrac{1}{2}(1+i\alpha_4,\tfrac{1}{2}(1-i)\alpha_4)]\ , \tag{3}$$

where

$$q_1=(1/2h)[(E_1-E)(E-E_5)]^{1/2}\ ,$$
$$a_1=\frac{1-i[(E_1-E)/(E-E_5)]^{1/2}}{1+i[(E_1-E)/(E-E_5)]^{1/2}}\ , \tag{4}$$
$$\alpha_4=\frac{\sqrt{2}\,(V_3^S+V_3^A)}{E_1-V_4^A-\frac{1}{2}h^2}\ .$$

The wave function through the second loop is given by

$$\phi_2=e^{-q_2 z}[(-i,1,0,0,\tfrac{1}{2}(1-i)\alpha_3,\tfrac{1}{2}(1+i)\alpha_3) + a_2(0,0,i,1,\tfrac{1}{2}(1-i)\alpha_3,\tfrac{1}{2}(1+i)\alpha_3)]\ , \tag{5}$$

where

$$q_2=(1/2h)[(E_3-E)(E-E_5)]^{1/2}\ ,$$
$$a_2=\frac{1-i[(E_3-E)/(E-E_5)]^{1/2}}{1+i[(E_3-E)/(E-E_5)]^{1/2}}\ , \tag{6}$$
$$\alpha_3=\frac{\sqrt{2}\,(V_3^S-V_3^A)}{E_3+V_4^A-\frac{1}{2}h^2}\ .$$

In (3) and (5) V_3^S, V_3^A, and V_4^A are the symmetric and antisymmetric pseudopotential form factors,[7] and z is the direction perpendicular to the surface. As stated above, in diamond crystals the conduction band is degenerate, giving rise to a degenerate loop $a_1\equiv a_2$; in this case the wave functions along the loop are usually written as $\frac{1}{2}(\phi_1+\phi_2)$ and $(1/2i)(\phi_1-\phi_2)$, ϕ_1 and ϕ_2 being the waves in (3) and (5), respectively.

The X_4 point is analyzed in an analogous way. Two wave functions (ϕ_3 and ϕ_4) are calculated after the analysis of the complex band structure at X_4; as they are similar to those given in (3) and (5), we shall omit details.

The bulk band structure at the R_1 point will be described by means of the plane waves

$$\begin{array}{ccccc}(\frac{1}{2},\frac{3}{2},0) & (\bar{\frac{3}{2}},\bar{\frac{1}{2}},0) & (\bar{\frac{1}{2}},\frac{1}{2},1) & (\bar{\frac{1}{2}},\frac{1}{2},\bar{1}) & (\frac{1}{2},\bar{\frac{1}{2}},0)\\ |\vec{\kappa}_1\rangle & |\vec{\kappa}_1\rangle & |\vec{\kappa}_3\rangle & |\vec{\kappa}_5\rangle & |\vec{\kappa}_2\rangle\end{array}\ . \tag{7}$$

The analysis of the complex band structure leads to a loop joining the valence band (E_2) to the conduction band (E_4). The wave function along this loop is given by

$$\phi_5=e^{-q_5 z}[(0,1,\tfrac{1}{2}i\gamma_1,\tfrac{1}{2}i\gamma_2,0)+a_3(\bar{1},0,\tfrac{1}{2}i\gamma_1,\tfrac{1}{2}i\gamma_2,0)]\ , \tag{8}$$

where

$$q_5=(1/2h)[(E_4-E)(E-E_2)]^{1/2}\ ,$$
$$a_3=\frac{1-i[(E_4-E)/(E-E_2)]^{1/2}}{1+i[(E_4-E)/(E-E_2)]^{1/2}}\ ,$$

and (9)

$$\gamma_1=\frac{\sqrt{2}\,(V_3^A+iV_3^S)}{E_4-\frac{3}{4}h^2}\ ,$$
$$\gamma_2=\frac{\sqrt{2}\,(V_3^A-iV_3^S)}{E_2-\frac{3}{4}h^2}\ .$$

The analysis of the real lines at R_2 gives rise to a single wave function ϕ_6 similar to that in (8). This function completes the set of six evanescent waves needed to perform the matching correctly.

We shall apply our analysis to the study of surface states at the semiconductor-vacuum interface. For the sake of simplicity we shall use the APM throughout. As stated elsewhere[5] this is not a reliable model as far as the calculation of surface-state energies is concerned; nevertheless, as we are interested in (a) checking our description of the evanescent wave functions by comparing our results with calculations which use that model (APM) and (b) understanding the role played by the ionic potential in the surface-state calculation, we shall use the APM everywhere in this section. In performing the surface-state calculation, the six wave functions described above (ϕ_i, $i=1,\ldots,6$) should be matched to six plane waves at the vacuum side.

A standard analysis gives rise to a secular equation which can be factored into the determinants

$$\det[D \pm (V_3^A/V_3^S)Z] = 0 , \tag{10a}$$

where D (diamond) and Z (zinc-blende) are the following matrices:

$$D = \begin{vmatrix} d_1 + id_2 & -d_1 + id_2 & d_5 \\ d_3 - id_4 & 0 & d_6 \\ 0 & d_3 + id_4 & -d_6 \end{vmatrix} \tag{10b}$$

and

$$Z = \begin{vmatrix} d_1 + id_2 & d_1 - id_2 & 0 \\ 0 & 0 & d_6 \\ 0 & 0 & d_6 \end{vmatrix} , \tag{10c}$$

where d_i, $i = 1, \ldots, 6$, are given by the following expressions:

$$\begin{aligned} d_1 &= [-\sqrt{2}\, V_3^S/2(E_1 - \tfrac{1}{2}h^2)](1 + a_1)(1 + \tfrac{1}{2}ih\mathfrak{L}_1) , \\ d_2 &= [\sqrt{2}\, V_3^S/2(E_1 - \tfrac{1}{2}h^2)](1 + a_1)(1 - \tfrac{1}{2}ih\mathfrak{L}_1) , \\ d_3 &= 1 - \tfrac{1}{2}ih\mathfrak{L}_3 , \\ d_4 &= -a_1(1 + \tfrac{1}{2}ih\mathfrak{L}_3) , \\ d_5 &= (1 - a_3) - ih\mathfrak{L}_1(1 + a_3) , \\ d_6 &= [\sqrt{2}\, V_3^S/(E_4 - \tfrac{3}{4}h^2)](1 + a_3) , \end{aligned} \tag{11}$$

with $\mathfrak{L}_i = (W_0 + \kappa_i^2 - E)^{-1/2}$, $i = 1, 3$ (W_0 fixes the vacuum level). In obtaining Eqs. (10) we have performed the following approximations: First, we have supposed the small splitting of the conduction band at the X point to be negligible, that is, $E_1 \sim E_3$ and $a_1 = a_2$ in expressions (3)–(6), and second, we have taken $V_4^A \sim 0$.

We want to stress that the secular equation (10a) gives rise to a degenerate surface state for covalent solids (diamond crystals), since in this case $V_3^A = 0$ and Eq. (10a) then becomes $[\det(D)]^2 = 0$. This agrees with previous theoretical analysis.[15,16] The ionic component V_3^A leads to an interaction between both surface states and then to the splitting of the two surface states, degenerate in the covalent limit. This shows, therefore, that Eq. (10a) includes clearly the heteropolar character of the (110) surface of zinc-blende solids.[17]

It is worthwhile studying the secular equation (10a) within the lowest approximation (two-band limit). This approximation consists in neglecting the (111) Fourier component of the crystal pseudopotential. In this case $d_1 = d_2 = d_6 = 0$, and Eq. (10a) can be factored in the following secular equations:

$$a_3 = (1 - ih\mathfrak{L}_1)/(1 + ih\mathfrak{L}_1) , \tag{12a}$$

$$a_1 = i(1 - \tfrac{1}{2}ih\mathfrak{L}_3)/(1 + \tfrac{1}{2}ih\mathfrak{L}_3) , \tag{12b}$$

$$a_1 = -i(1 - \tfrac{1}{2}ih\mathfrak{L}_3)/(1 + \tfrac{1}{2}ih\mathfrak{L}_3) , \tag{12c}$$

which correspond, respectively, to three one-dimensional models.[18] The meaning of Eqs. (12) can be clearly understood. Equation (12a) is related to the loop at the R_1 point and therefore corresponds to a one-dimensional model in which the bulk band gap at R_1 is described by means of an effective pseudopotential Fourier component $V_{\text{eff}}(220)$; in this approximation we retain the energy levels calculated by means of more elaborate models,[7] in the spirit that our approach describes the essential features of the wave functions and thus of the matching process. Equations (12b) and (12c) are typical for a two-dimensional system[18,19] and are related to the two loops of the complex band structure at X. In this approximation we have decoupled the points X and R in such a way that a surface state could appear at one of these points for energies corresponding to the allowed energy region at the other point; in such a case the interaction between both points, introduced by the (111) pseudopotential Fourier component, would change the surface state into a resonance. Finally, we stress that this approximation does not take into account the heteropolar character of the solid as the $V(220)$ form factor is purely covalent and all information on the ionic character of the pseudopotential is contained in the (111) Fourier component neglected here.

B. Point $\bar{\Gamma}$

Two points of high symmetry of the bulk band structure project into $\bar{\Gamma}$ [Fig. 1(b)], $\Gamma(000)$ and $X(110)$. A standard calculation gives the lines of real energy and the wave functions along them. Figure 2 shows the real lines in the region of the fundamental gap. Omitting details, we shall restrict ourselves to the discussion of the secular equations for surface-state energies in the lowest approximation (two-band model). As discussed in Sec. II A, this approximation consists in neglecting the terms involving the (111) form factors. We shall describe just the Σ_1 symmetry which is the only one giving surface states.[6] For this symmetry the surface states are given by

$$b_1 = (1 - ih\mathfrak{L}_0')/(1 + ih\mathfrak{L}_0') , \tag{13a}$$

$$b_2 = (1 - ih\mathfrak{L}_1')/(1 + ih\mathfrak{L}_1') , \tag{13b}$$

where

$$b_1 = \frac{1 - i[(E_2' - E)/(E - E_3')]^{1/2}}{1 + i[(E_2' - E)/(E - E_3')]^{1/2}} , \tag{14a}$$

$$b_2 = \frac{1 - 2i[(E_5' - E)/(E - E_4')]^{1/2}\{[\frac{1}{2}(E_5' + E_6') - E]/(E_6' - E)\}^{1/2}}{1 + 2i[(E_5' - E)/(E - E_4')]^{1/2}\{[\frac{1}{2}(E_5' + E_6') - E]/(E_6' - E)\}^{1/2}} , \tag{14b}$$

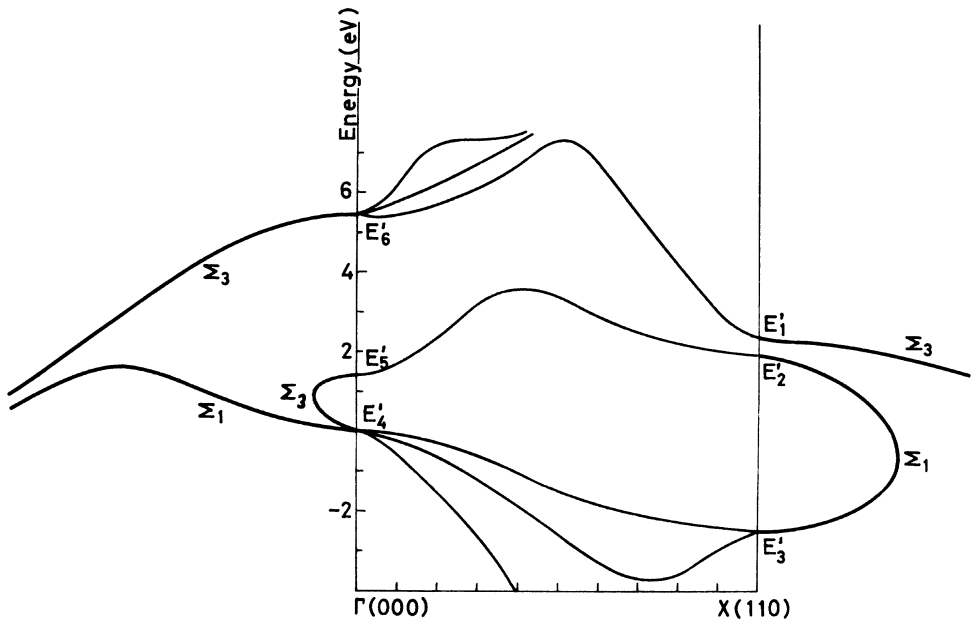

FIG. 2. Real lines of GaAs, along the Γ(000)–X(110) direction, included in the analysis of the $\bar{\Gamma}$ point. The symmetries attached to the lines of real energy are those corresponding to the diamond lattice (see text).

while the $\mathcal{L}_i'$ are

$$\mathcal{L}_0' = (W_0 - E)^{-1/2} \quad \text{and} \quad \mathcal{L}_1' = (W_0 + \kappa_1'^2 - E)^{1/2} ,$$

$|\kappa_1'\rangle = (0, 1)$. The energy levels $E_1', \ldots, E_6'$ (X_5, X_1, X_3, Γ_{15}, Γ_1, and Γ_{15} in the usual terminology) are specified in Fig. 2. In the covalent limit Eq. (13a) corresponds to the Σ_1 symmetry[20] whereas Eq. (13b) belongs to the symmetry Σ_3. The meaning of these equations is clear. The first equation is associated to the loop at the X point (Fig. 2), while Eq. (13b) is associated to the loop at Γ (Fig. 2). This can be seen in a clearer way by noting that the level E_6' is, in ionic crystals, at much higher energies than E_4' and E_5', in such a way that

$$b_2 \simeq \frac{1 - \sqrt{2}\, i[(E_5' - E)/(E - E_4')]}{1 + \sqrt{2}\, i[(E_5' - E)/(E - E_4')]} .$$

Finally, we stress that the fact that the lowest approximation decouples the loops at X and Γ implies that we could obtain surface states below the fundamental gap,[15] in the energy region $E' \leq E \leq E_4'$; however, in higher approximations such a surface state would emerge into a resonance state.

C. Surface-state energies and discussion of the approximations

In order to check the approximations we have performed in describing the semiconductor evanescent wave functions, we have calculated surface-state energies for seven zinc-blende compounds; this calculation allows us to compare our results with those obtained by means of more elaborate approaches, in particular the calculation of Ball and Morgan.[6] In Table I we report our results (points $\bar{\Gamma}$ and $\bar{X}$) and those obtained by Ball and Morgan; the agreement between both theoretical calculations is greater for the $\bar{\Gamma}$ point. This seems reasonable since in this point we have described the evanescent wave functions by means of more parallel components $|\vec{\kappa}\rangle$ than in the case of $\bar{X}$. Note that at the $\bar{\Gamma}$ point of GaAs we have found a single surface state, whereas Ball and Morgan find two surface states; the reason is that those authors obtain the surface state close to the top of the valence band, while in our case the surface state is just appearing.

Finally, it is worth noting that the point $\bar{X}$ could be a measure of the ionic character of the solid; as discussed previously in this section, Eq. (10a) gives the surface states which are degenerate in the covalent limit and split in the ionic limit. The results obtained with that equation are reported in Table I and display an increasing gap on going from less to more ionic crystals; in other words, as the ratio V_3^A/V_3^S increases.

Our results for surface-state energies indicate that our description of the semiconductor evanescent wave functions is good enough for the particular case we shall study in Sec. III, namely, the continuum density of states characteristic of junctions with metals of high density (Al). This point will be cleared up in Sec. IV.

III. ELECTRONIC STATES AT METAL-SEMICONDUCTOR INTERFACE

In this section we shall discuss the characteristics of the interface states at the M-S junction.

TABLE I. Surface-state energies (eV) at the points $\bar{\Gamma}$ and $\bar{X}$ of the two-dimensional BZ of the (110) zinc-blende surface for some crystals. In the cases of GaAs and InP, (a) corresponds to Ref. 6 and (b) to the present calculation; the results for all of the other solids are those calculated in this work. The energies are referred to the top of the valence band for each semiconductor.

	GaAs		InP						
	(a)	(b)	(a)	(b)	GaP	InSb	CdTe	ZnSe	ZnS
$\bar{\Gamma}$	0.272	···	0.272	0.05	0.05	0.35	1.05	0.85	0.8
	1.088	0.8	1.224	0.9	1.3	0.4	1.2	1.6	2.2
$\bar{X}$	0.544	1.0	0.408	0.9	0.92	0.9	−0.06	−0.2	−0.1
	1.088	1.48	1.088	1.44	43	1.37	2.02	2.4	2.55

The metal will be described by the Sommerfeld model. Depending on the width of the metallic band we shall find different types of interface states; namely, virtual states[3] for metals of high density, Breit-Wigner resonances[3] for narrow-band metals, and even true surface states for metals of very narrow band. All of these cases will be discussed by means of particular examples for the points $\bar{X}$ and $\bar{\Gamma}$ and for junctions with different types of metals. At the end of this section we shall discuss the relevance of the interface potential for the density of interface states at the M-S junction.

In order to investigate the density of interface states we shall use the surface-Green's-function method.[21] In this scheme the density of interface states minus the density of states associated with the hard cores of both media is directly given by (for a given $\vec{\kappa}$)

$$\rho(E,\vec{\kappa}) = -\frac{1}{\pi}\frac{d}{dE}\arg\det \mathcal{G}_s^{-1}(E^+) \ , \tag{15}$$

where $\mathcal{G}_s^{-1}$ is the inverse matrix of the surface Green's function (see Ref. 21 for details). There are many ways to calculate $\mathcal{G}_s$; once we have analyzed the semiconductor evanescent wave functions and the matching at the interface, the most straightforward way to calculate $\mathcal{G}_s$ is to get it from the secular equation obtained through the matching at the interface.[22] Nevertheless, to avoid details we shall derive the determinant of $\mathcal{G}_s^{-1}$ in an heuristic way.

A. Point $\bar{X}$

The surface-state energies were calculated by means of Eq. (10a). Keeping in mind the definition of $\rho(E)$ in (15), the density of states is

$$\rho(E,\bar{X}) = -\frac{1}{\pi}\frac{d}{dE}\arg\det\left(D \pm \frac{V_3^A}{V_3^S}Z\right) + \frac{1}{\pi}\frac{d}{dE}\arg\det\left(D^0 \pm \frac{V_3^A}{V_3^S}Z^0\right) \ , \tag{16}$$

where D^0 and Z^0 are the matrices D and Z calculated by setting $\mathfrak{L}_i = 0$ in Eq. (11), that is, the semiconductor joined to an infinite potential barrier (hard core). It is worth noting that the right-hand side of (16) includes contributions coming from possible surface states associated with the infinite-barrier case (hard-core surface states); these contributions should be neglected as they cancel with the other terms involved in the definition of $\rho(E)$,[21,23] which we have omitted.

In this case we shall also analyze in detail the lowest approximation (two-band limit), since, in this limit, Eq. (16) factors into three terms,

$$\rho(E,\bar{X}) = \rho_1 + \rho_2 + \rho_3 \ , \tag{17}$$

where

$$\rho_1(E) = -\frac{1}{\pi}\frac{d}{dE}\arg\frac{a_3 - (1 - ih\mathfrak{L}_1)/(1 + ih\mathfrak{L}_1)}{a_3 - 1} \ , \tag{18a}$$

$$\rho_2(E) = -\frac{1}{\pi}\frac{d}{dE}\arg\frac{a_1 - i(1 - \frac{1}{2}ih\mathfrak{L}_3)/(1 + \frac{1}{2}ih\mathfrak{L}_3)}{a_1 - i} \ , \tag{18b}$$

$$\rho_3(E) = -\frac{1}{\pi}\frac{d}{dE}\arg\frac{a_1 + i(1 - \frac{1}{2}ih\mathfrak{L}_3)/(1 + \frac{1}{2}ih\mathfrak{L}_3)}{a_1 + i} \ . \tag{18c}$$

In the case of semiconductor-vacuum interfaces, it is clear that Eqs. (17) give the density associated with the surface states calculated by means of Eq. (10a) minus that quantity associated with the infinite-barrier case (hard cores).

Equations (17) allow a straightforward discussion of the different types of interface states one can find at the M-S junction. In those equations, the magnitudes $\mathfrak{L}_1$ and $\mathfrak{L}_3$ can be either imaginary or real quantities, telling us whether the wave propagates or does not propagate, respectively, at the metal side. If the metallic band is wide enough, both quantities will be imaginary, giving a continuous density of virtual states along the forbidden gap (Fig. 3) and displaying no structure (this is the case usually analyzed[3,24,25]); the total density of states is $\frac{1}{2}$ for each loop. If the metal has a narrow band, it could happen that $\mathfrak{L}_3$ would

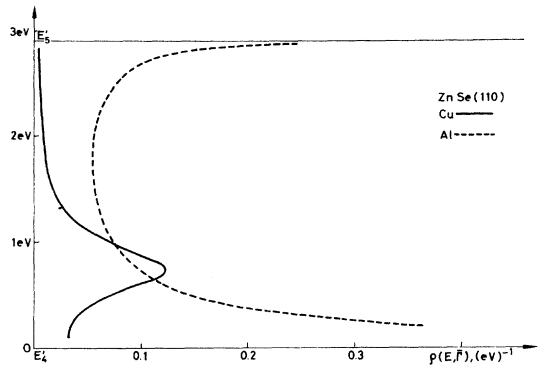

FIG. 3. Broken line: density of virtual states for the Al-ZnSe(110) junction. Solid-line: Breit-Wigner resonance characteristic of the junction Cu-ZnSe(110). The results correspond to the σ_3 symmetry of the $\bar{\Gamma}$ point.

be real and $\mathfrak{L}_1$ imaginary. In this case we would find "true surface states" for the loops associated with the X points and a density of virtual states for the R points; then, if we introduce the interaction between X and R, we find a resonance state of the Breit-Wigner type (Fig. 3). In the last case, the total density of states is one-half of the virtual state and one true surface state. In Fig. 4 we plot, for the junction ZnS-Pt, two distinct energy regions at the $\bar{X}$ point; in region II we can find resonance surface states and in region III true surface states. These features of the density of states at the M-S junction indicate that the characteristics of the contact depend on the particular metal.

B. Point $\bar{\Gamma}$

The lowest approximation at this point allows us to write the density of interface states, as in $\bar{X}$, in the following form:

$$\rho(E,\bar{\Gamma}) = \rho_1 + \rho_2 + \rho_3 \ , \tag{19}$$

where in this case the terms ρ_i, $i = 1, 2, 3$, are given by

$$\rho_1(E) = -\frac{1}{\pi}\frac{d}{dE}\arg\frac{b_1 - (1 - ih\mathfrak{L}_0')/(1 + ih\mathfrak{L}_0')}{b_1 - 1} \ , \tag{20a}$$

$$\rho_2(E) = -\frac{1}{\pi}\frac{d}{dE}\arg\frac{b_2 + (1 - ih\mathfrak{L}_1')/(1 + ih\mathfrak{L}_1')}{b_2 + 1} \ , \tag{20b}$$

$$\rho_3(E) = -\frac{1}{\pi}\frac{d}{dE}\arg\frac{b_3 - (1 - ih\mathfrak{L}_1')/(1 + ih\mathfrak{L}_1')}{b_3 - 1} \ . \tag{20c}$$

In this case we can also have the types of interface states discussed in Sec. IIIA. The virtual states appear for the loop associated with the parallel component of the crystal momentum of lowest energy (that is, b_1), while for the loops b_2 and b_3 we can find true surface states. As in $\bar{X}$, the interaction between the loops b_1, b_2, and b_3 lead to a resonance of the Breit-Wigner type (Fig. 3). In Fig. 4 we have sketched the situation for the junction ZnS-Pt; in this case we have at $\bar{\Gamma}$ an energy region where one can find virtual states (region I of Fig. 4) and a much larger region (II of Fig. 4) where resonance states can be obtained. These features of the density of interface states indicate, as in $\bar{X}$, that the characteristics of the contact can depend on the particular metal.

As we are interested in the role played by the ionic character of the semiconductor at the M-S junction we shall restrict ourselves to junctions with metals of high density, for which the analysis of the density of interface states is much simpler. In Table II we have reported our results for the density of interface states for junctions of several zinc-blende crystals (InSb, GaAs, InP, GaP, CdTe, ZnSe, and ZnS) with Al; the calculation has been done for an energy which is $\epsilon_0 = \frac{1}{3}E_g$, where the energy refers to the top of the valence band and E_g is the thermal gap for each semiconductor (this energy is where the Fermi level is supposed to be placed for most of the junctions,[1] as will be discussed in Sec. IV). Although we have performed our calculation by means of the highest approximation we have studied, it is worth pointing out that the density of states does not vary very much (20%)

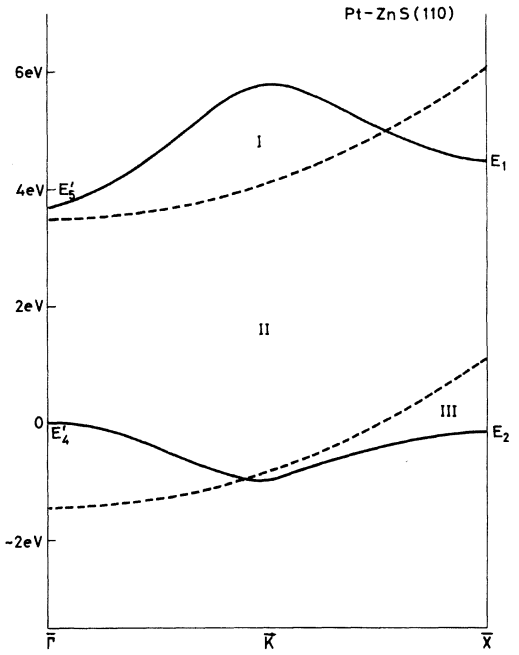

FIG. 4. Bulk band structure of ZnS projected on the (110) face (solid line) and the two free electron parabolas (see text) of lowest energy for Pt (broken line). Different regions are to be noted: in region I only virtual states can be found, whereas in regions II and III resonances or true surface states, respectively, can be obtained.

if we use the two-band model. This is in contrast to the case of the semiconductor-vacuum system, where both approximations differ qualitatively [at $\bar{X}$ the lowest approximation gives degenerate surface states, while the highest approximation splits those states by an amount proportional to the ionic character of the crystal; see Eq. (10a)]. As a consequence, the density of interface states is not directly a function of the ionic potential but only of the band effective masses and of the magnitude of the forbidden gap (both quantities are functions of the strength of the atomic potential). Although the calculated density of states decreases as the ionic character of the solid increases, the differences between the densities corresponding to GaAs and ZnS (Table II) are not as large as one could expect from the experimental data.[1,26] One feature to be noted is the slight difference between the densities calculated at the $\bar{\Gamma}$ point and at the $\bar{X}$ point; this independence of $\rho(E, \vec{\kappa})$ from the particular $\vec{\kappa}$ has also been found for the Si(111)-Al junction.[22] As a final remark, we stress that these features are also valid for all junctions with metals of high density; the density of states being, in this case, almost independent of the particular metal.

C. Interface potential

So far we have assumed the APM; the question now is the quality of this model for the M-S junction. We know that for the study of the free surface of semiconductors the APM is a poor model,[5] at least for the electronic surface-state energies, which are very sensitive to the profile of the potential at the surface.

In order to elucidate this point we have studied a model with the following features: (a) As we shall study only the case of metals with a wide Sommerfeld band, the model displays a density of "virtual states"; (b) we shall use a one-dimensional model; this point is justified by the reliability of the lowest approximation, as discussed earlier; and (c) we shall use a linear barrier as a model of the interface potential.[27,28]

TABLE II. Density of interface states (eV^{-1}) at the metal (al)–(110-zinc-blende junction for some semiconductors. The density of states has been calculated for an energy equal to $\frac{1}{3} E_g$, referred to the top of the valence band, where E_g is the thermal gap for each semiconductor. Results are given for the points $\bar{\Gamma}$ and $\bar{X}$ of the two-dimensional BZ.

	$\bar{\Gamma}$	$\bar{X}$
GaP	0.224	0.43
GaAs	0.348	0.49
InSb	0.88	0.62
InP	0.38	0.46
CdTe	0.28	0.40
ZnSe	0.185	0.33
ZnS	0.117	0.29

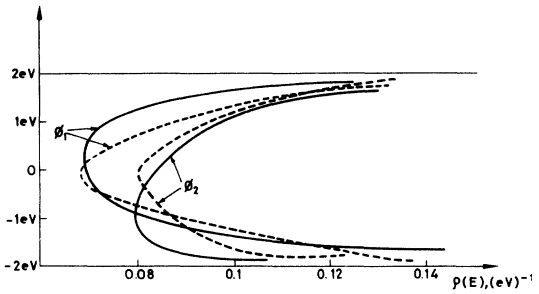

FIG. 5. Density of virtual states at the M-S junction for a one-dimensional model, calculated using either the APM (broken line) or the linear-barrier model (solid line). Two cases are shown: $\phi_1 = 180°$ and $\phi_2 = 0°$, that is, the periodic potential is finished at a minimum (bonding case) or a maximum (antibonding case), respectively (see Ref. 5).

We have studied the density of virtual states for a semiconductor like GaAs and a metal of a Sommerfeld band of 5.0 eV; we then varied the slope of the linear potential and thus the width of the interface region. The results for two extreme cases are drawn in Fig. 5. We have used an interface region 8 Å wide; this is clearly unphysical but it amounts to a test which is even stricter than physical reality. The results show that the densities of virtual states of the Fermi level corresponding to that model and to the APM do not differ by more than 5%. Moreover, the total density of states at the semiconductor gap is nearly independent of the interface potential, the differences being negligible. Our conclusion, then, is that the density of interface states is not very sensitive to interface potential, justifying in this way the calculations we have performed in this section.

IV. CALCULATION OF THE BARRIER HEIGHT: COMPARISON WITH EXPERIMENTAL DATA

In order to obtain the relation between the barrier height at the junction and the metal work function, we shall follow the work of Cowley and Sze.[26] First, we consider the experimental data reported by Mead,[29] according to which the Fermi level for several dielectrics in contact with Au is placed, as stated in Sec. III, at $E_F = \frac{1}{3} E_g$. (A theoretical calculation of the Fermi level at the junction would require a complete analysis of the charge redistribution throughout the whole spectrum of occupied states.[23,24]) The fact that the density of interface states, D, is almost independent of the metal (for metals of high density), and that the distance δ between these (virtual) interface states and the opposed charge placed at the metal surface is also independent of the particular metal, as will be discussed later, allow us to write the barrier height

TABLE III. Calculated values of the slope S and the electronic density of resonance surface states for different III-V and II-VI compounds. The density of resonance surface states has been calculated for an energy referred to the top of the valence band equal to $\frac{1}{3}E_g$, where E_g is the thermal gap for each semiconductor.

	InSb	GaAs	InP	GaP	CdTe	ZnSe	ZnS
$10^{-14}D$ (eV^{+1} cm^{+2})	5.05	3.72	3.45	3.12	2.34	2.28	1.96
S	0.05	0.1	0.09	0.12	0.14	0.155	0.18

ϕ_{Bn} (for type n semiconductors) at the junction as a linear function of the metal workfunction[26] ϕ_M:

$$\phi_{Bn} = S\phi_M + b \ , \tag{21}$$

where

$$S = (1 + 4\pi D\delta e^2)^{-1} \ , \tag{21a}$$

b is a constant which can be determined through experimental measurements[29] and e is the electron charge.

In Sec. III we discussed the calculation of the density of interface states for seven zinc-blende solids joined to a metal of high density (Al). As shown in Table I, the density of interface states does not depend very much on the particular $\vec{\kappa}$. This allows us to calculate the total density of states for a given energy in the following way:

$$D(E_F) = \frac{1}{N}\sum_{\vec{\kappa}} \rho(\vec{\kappa}, E_F) \ , \tag{22}$$

where, in the present case, the sum over $\vec{\kappa}$ is restricted to $\bar{\Gamma}$ and $\bar{X}$, and where N is the number of terms included in the sum (in this case $N = 2$).

In Table III we have reported our results for the total density of states. As pointed out in Sec. III, this density decreases as the ionic character of the solid increases; nevertheless, the difference between the densities corresponding to the covalent solid (GaAs) and those found for the ionic crystals (ZnS) are not as large as expected from experimental measurements.[26]

We shall now discuss how to calculate the effective distance between the virtual states and the opposed charge at the metal surface, which will complete the information needed to calculate the slope S of Eq. (21). In order to estimate δ, let us first consider the screening of the resonance charge placed at the semiconductor half-space. We assume that this screening can be described by a bulk electronic dielectric function; in particular we shall use that proposed by Inkson[30] (which is a simplified version of that given by Penn[31])

$$\epsilon_S = 1 + \frac{\epsilon_\infty - 1}{1 + (\epsilon_\infty - 1)k^2/k_s^2} \ , \tag{23}$$

where k_s and ϵ_∞ are the Fermi-Thomas wave vectors and the static dielectric constant, respectively. Bearing in mind that the resonance charge decays as $\exp(-2q|z|)$, where q is directly obtained from the equations of the loops discussed in Sec. II, and symmetrizing into the whole space,[32] the effective distance from the charge to the semiconductor surface turns out to be approximately $1/k_s + 1/2\epsilon_\infty q$. We may suppose that the screening of the induced charge in the metallic side is described by the usual dielectric function

$$\epsilon_m = 1 + k_m^2/k^2 \ , \tag{24}$$

where k_m is the Fermi-Thomas wave vector of the metal. Finally, we obtain the total effective distance to be inserted into (21),

$$\delta = \frac{1}{2\epsilon_\infty q} + \frac{1}{k_s} + \frac{1}{k_m} \ . \tag{25}$$

This expression indicates that the effective distance is a sum of a distance $(k_s^{-1} + k_m^{-1})$ within which there is no screening of the charge plus the distance $1/2\epsilon_\infty q$ which is nothing but the effective distance where the charge, completely screened by the crystal, is located.

This result allows us to include the effect of the ionic screening. Since the effective distance related to the ionic screening [this distance is characterized by the distance between equivalent (110) planes in the solid] can be expected to be larger than k_s^{-1}, we can write δ as follows:

$$\delta \approx \frac{1}{2\epsilon_0 q} + \frac{1}{k_s} + \frac{1}{k_m} \ , \tag{26}$$

where ϵ_0 includes the ionic screening in the long-wavelength limit.

The value of $k_s^{-1} + k_m^{-1}$ is very approximately 1 Å and is largely independent of the particular metal, as was assumed at the beginning of this section. The term $1/2\epsilon_0 q$ can be calculated as follows: As discussed in Sec. III, the density of virtual states can be calculated by considering the different loops, included in the analysis independently; this allows us to attach to each loop an effective distance related to the imaginary part of the component of the crystal momentum perpendicular to the surface, q. The value of δ does not depend very much on the particular semiconductor since (a) the value of $k_s^{-1} + k_m^{-1}$ dominates and (b), on the other hand,

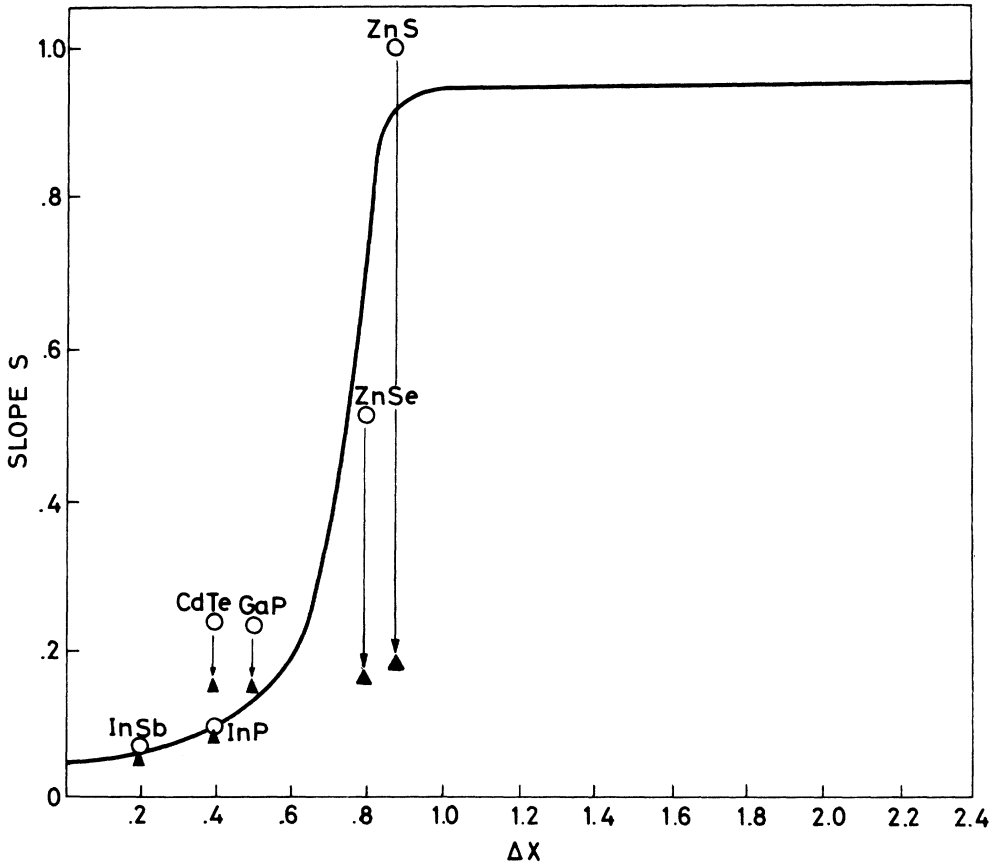

FIG. 6. Theoretical values (▲) and experimental data (○) for the slope S plotted as a function of the lattice electronegative difference ΔX. The curve is taken from Ref. 2.

$(\epsilon_0 q)^{-1}$ is almost constant because as the ionic character of the crystal increases, ϵ_0 decreases and q increases, keeping the value of $E_F q$ almost constant.

Now we are able to calculate the magnitude $D\delta$ as the sum of the charges associated with each loop included in the particular $\vec{\kappa}$ under study, multiplied by the effective distance associated to that loop. Thus $D\delta$ for the energy E_F is just

$$D\delta(E_F) = \frac{1}{N}\sum_{\vec{\kappa},i}^{N} \rho(\vec{\kappa}, i; E_F)\delta(\vec{\kappa}, i; E_F) \ , \qquad (27)$$

where N is the number of $\vec{\kappa}$ considered and i runs over the loops included in the analysis of each $\vec{\kappa}$. In our case $N=2$, and the $\vec{\kappa}$ are $\bar{X}$ and $\bar{\Gamma}$.

Our results for the slope S are given in Table III. The theoretical values of the slope are plotted in Fig. 6, together with the experimental data collected by Kurtin *et al.*[2] The present results differ slightly from those reported in I, because in that case we included just one point in the analysis ($\bar{\Gamma}$). The inclusion of $\bar{X}$ has increased the values of the total density of interface states and then lowered the values of S; nevertheless, the discrepancies are not considerable. As in I, there is an excellent agreement between theory and experiment for crystals of the covalent group (InSb, GaAs, and InP) and the discrepancy between theory and experiment increases with increasing ionicity (ZnS).

V. CONCLUDING REMARKS

In this paper we have presented a study of the properties of the (110) zinc-blende surfaces and of their junction with different metals. Although our main purpose was the analysis of the covalent-ionic transition in the M-S interface, the study of the free surface which we have carried out has allowed us to analyze clearly the heteropolar character of the (110) surface. Regarding the interface density of states for junctions with metals of high density, we have proved that the lowest approximation gives quite accurate results; this conclusion shows that since this approximation does not involve the (111) pseudopotential form factors, the ionic character of the crystal is not of prime relevance in calculating densities of virtual states.

As for the covalent-ionic transition, we have found that our model, based on a one-electron

scheme within the pseudopotential framework, is unable to explain the data reported by Kurtin *et al.*[2]; our model fails in treating highly ionic compounds. Since the slope S calculated in this paper is nearly independent of the ionic character of the solid, one can ask whether the agreement between theory and experiment for covalent solids is fortuitous, the one-electron model being basically inadequate for the study of metal-semiconductor junctions. Nevertheless, it should be noted that the covalent-ionic transition has been observed in different kinds of experimental properties, as discussed by Kurtin *et al.*[2] Their results regarding optical absorption (excitons and nondirect transitions) tend to show that the one-electron approach is not a proper scheme for the study of properties of ionic solids. We think that the experimental data reported by Kurtin *et al.*,[2] the model discussed in this paper, and other theoretical works about many-body effects in ionic solids[33] point in the same direction; namely, they show that the one-electron scheme is an adequate framework for the treatment of some properties of covalent solids, but cannot explain most of the characteristics of the ionic solids (the correlation effects are greatly enhanced as the ionicity of the solids, and then the localization of the electrons, increases). Hence we think that the metal-ionic junctions should be studied by including many electron effects and, of course, the entire charge of the system, that is, the valence electrons[34] and the resonance surface states.

ACKNOWLEDGMENTS

We are indebted to Dr. F. García-Moliner and Dr. J. Rubio for many useful discussions and for the critical reading of the manuscript.

---

*Present address: Department of Physics, University of California, Berkeley, Calif. 94720.

[1]S. M. Sze, *Principles of Semiconductor Devices* (Wiley, New York, 1969).
[2]S. Kurtin, T. C. McGill, and C. A. Mead, Phys. Rev. Lett. 22, 1433 (1969).
[3]V. Heine, Phys. Rev. 138, A1689 (1965).
[4]F. Flores, E. Louis, and F. Yndurain, J. Phys. C 6, L465 (1973), hereafter referred as I.
[5]F. Flores, E. Louis, and J. Rubio, J. Phys. C 5, 3469 (1972).
[6]G. Ball and D. J. Morgan, Phys. Status Solidi B 50, 199 (1972).
[7]M. L. Cohen and T. K. Bergstresser, Phys. Rev. 141, A789 (1966).
[8]V. Heine, Proc. Phys. Soc. Lond. 81, 300 (1963).
[9]M. Elices, F. Flores, E. Louis, and J. Rubio, J. Phys. C 7, 3020 (1974).
[10]This has been proved to work also for the (111) surface of zinc-blende crystals (see Ref. 11). Nevertheless, we are aware of the important differences between that surface and the (110), which could be of primary importance in choosing the approximations to describe the evanescent waves.
[11]E. Louis and M. Elices, Phys. Rev. B 12, 618 (1975).
[12]Points of two-dimensional symmetry will be denoted by capital letters with bars above them.
[13]Hereafter we shall write the plane waves in units of $2\pi/a$, a being the lattice constant.
[14]V. Heine and R. O. Jones, J. Phys. C 2, 719 (1969).
[15]R. O. Jones, Phys. Rev. Lett. 20, 992 (1968).
[16]F. Yndurain and M. Elices, Surf. Sci. 29, 540 (1972).
[17]The heteropolar character of the (110) surface has been previously introduced, although in a rather simplified fashion, by E. Louis and F. Yndurain (see Ref. 25).
[18]F. Flores and J. Rubio, J. Phys. C 6, L258 (1972).
[19]F. Forstmann, Z. Phys. 235, 69 (1970).
[20]R. O. Jones, Ph.D. thesis (University of Cambridge, 1966) (unpublished).
[21]F. García-Moliner and J. Rubio, J. Phys. C 2, 1789 (1969).
[22]J. Rubio, F. Flores, and E. Louis (unpublished).
[23]C. Tejedor, E. Louis, and F. Flores, Solid State Commun. 15, 587 (1974).
[24]F. Yndurain, J. Phys. C 4, 2849 (1971).
[25]E. Louis and F. Yndurain, Phys. Status Solidi B 57, 175 (1973).
[26]A. M. Cowley and S. M. Sze, J. Appl. Phys. 36, 3212 (1966).
[27]The use of the linear barrier to describe the interface potential has been justified for the semiconductor-vacuum system (see Ref. 28).
[28]E. Larrea and F. Flores, Surf. Sci. 49, 339 (1975).
[29]C. A. Mead, Solid State Electron. 9, 1023 (1966).
[30]J. C. Inkson, J. Phys. C 5, 2599 (1972).
[31]D. R. Penn, Phys. Rev. 128, 2093 (1962).
[32]F. Flores, Nuovo Cimento B 14, 1 (1973).
[33]S. T. Pantelides, D. J. Mickish, and A. B. Kunz, Phys. Rev. B 10, 2602 (1974).
[34]A. J. Bennett and C. B. Duke, Phys. Rev. 162, 578 (1967).